JOURNAL OF SOLID STATE CHEMISTRY 75, 147–155 (1988)

Preparation, Crystal Structures, and Electronic Properties of $LiGaCl_3$ and $LiGaI_3$

WOLFGANG HÖNLE, GORDON MILLER, AND ARNDT SIMON

Max-Planck-Institut für Festkörperforschung, Heisenbergstrasse 1, 7000 Stuttgart 80, West Germany

Received October 19, 1987; in revised form January 25, 1988

$LiGaCl_3$ and $LiGaI_3$ have been prepared from LiX and GaX_2 in sealed glass ampoules at 470 and 540 K, respectively. The crystal structures have been determined using single crystals ($LiGaCl_3$: a = 1513.7(3) pm, b = 973.0(2) pm, c = 613.2(2) pm, $Pnma$, Z = 8; $LiGaI_3$: a = 846.7(3) pm, b = 1137.2(3) pm, c = 713.2(2) pm, β = 91.77(5)°, $P2_1/m$, Z = 4). $LiGaCl_3$ is a new structure type, whereas $LiGaI_3$ is isotypic to $LiGaBr_3$. Both structures are characterized by eclipsed Ga_2X_6 units with d(Ga–Ga) = 239.1 pm (chloride) and 242.8 pm (iodide). The arrangement of the trigonal prisms, $(Ga_2)X_6$, is similar to that in SrAg and $GdFeO_3$ for the chloride and iodide respectively. The lengthening of the Ga–Ga bond distance in the sequence Cl to I can be rationalized in terms of increasing population of the Ga_2 σ^* levels as the electronegativity of the anion decreases.

1. Introduction

For the reduced gallium halides, $M^{I}GaBr_3$ (M = Li^+, Ga^+), we have shown that in both cases $Ga_2Br_6^{2-}$ dianions exist in an eclipsed conformation. We already indicated that there is no significant difference in the experimentally determined Ga–Ga bond length for the staggered and eclipsed conformation (*1–3*). Since only a staggered conformation for $Ga_2[Ga_2I_6]$ has been found to date, we were interested in whether an eclipsed conformation could also be verified in the cases of $LiGaCl_3$ and $LiGaI_3$. We report here on the preparation, the crystal structures, and the electronic structures of LiGaX_3 (X = Cl, I).

2. Preparation

The preparation has already been reported in detail and follows the procedures outlined there (*1, 2*). The reduced binary gallium halides, Ga_2X_4 (X = Cl, I) were melted together with LiX (X = Cl, I) in equimolar portions under inert conditions in closed solidex ampoules at 473 K ($LiGaCl_3$) and 543 K ($LiGaI_3$). The sample weights were approximately 1.3 g ($LiGaCl_3$) and 1.9 g ($LiGaI_3$).

3. Properties

$LiGaCl_3$ crystallizes in the form of colorless platelets, which melt congruently at 456 K according to DTA experiments (sealed quartz ampoules, NETZSCH 404 S, heating/cooling at 10 K/min, samples ~80 mg, sealed under 1 bar Ar). $LiGaI_3$ crystallizes as a light yellow colored compound with no preferred morphology. Its melting point is 528 K. Both compounds hydrolyze in wet air yielding dark oxidation products. For both compounds the DTA experiments

0022-4596/88 $3.00

TABLE I

CRYSTALLOGRAPHIC DETAILS FOR $LiGaCl_3$ AND $LiGaI_3$

Formula; molar mass (a.m.u.)	$LiGaCl_3$; 183.02	$LiGaI_3$; 457.37
Lattice constants (295 K)	a = 1513.7(3) pm	a = 846.7(3) pm
from refined 2Θ-values of	b = 973.0(2) pm	b = 1137.2(3) pm
12 *hkl* ($20° \leq 2\Theta \leq 25°$)	c = 613.2(2) pm	c = 713.2(2) pm
		β = 91.77(5)°
Lattice constants from modified	a = 1519.9(4) pm	a = 854.1(4) pm
Guinier powder photographs	b = 981.7(4) pm	b = 1151.9(6) pm
($CuK_{\alpha 1}$ = 154.056 pm)	c = 614.8(2) pm	c = 718.5(4) pm
		β = 91.89(4)°
T(K); $n(hkl)$	403; 32	463; 15
Space group (No.); Z	*Pnma* (No. 62); 8	$P2_1/m$ (No. 11); 4
d_c(g/cm³) V_M(cm³/mol)	2.691; 68.00	4.426; 103.24
Intensity measurement	Nicolet $R3$, $2\Theta_{max} \leq 55°$; four-circle diffractometer with variable scan speed; ω-scan; Mo$K\alpha$ (71.073 pm); graphite monochromator; scintillation counter; empirical absorption correction with 12 *hkl* in ψ-scan mode	
Structure solution, refinement	Direct methods in SHELXTL (*5*); SOLV 1.2; 300 phases; 5999 TPR	Starting parameter of $LiGaBr_3$[1]
$N(hkl)$; $N'(hkl)$ with $I > 3\sigma(I)$	1239; 1030	1760; 1508
n (variables)	53	56
R_{iso}; R_{aniso}; $R_{all\ hkl}$	0.059; 0.037; 0.038	0.112; 0.052; 0.056
R_w, $w = 1/\sigma^2$; goodness of fit	0.037; 2.89	0.055; 4.39

revealed small endothermic effects at 377 K ($LiGaCl_3$) and 445 K ($LiGaI_3$) with a hysteresis of approximately 20 K on cooling. X-ray powder patterns taken with the modified Guinier technique (*4*) clearly demonstrate that no structural phase transitions occur at these temperatures. In the pattern of the $LiGaCl_3$ sample weak lines of $LiGaCl_4$ were present at room temperature, which were absent at 403 K. The observed thermal effect before the melting of the compound is thus assigned to eutectic melting for the chloride and should have the same origin for the iodide.

4. Structure Determinations

Single crystals were selected in a glove box with an integrated microscope and were fixed in glass capillaries with baked out silicon grease. Testing of the crystal quality, determination of approximate lattice constants, and determination of the extinction relations were performed using precession photographs as well as axial photographs on the four circle diffractometer. Further crystallographic details are collected in Table I. Calculated powder patterns (*6*) show good agreement between observed and calculated intensities. Table II contains the positional and thermal parameters for the atoms in the two structures.

5. Extended Hückel MO Calculations

The electronic structure and chemical bonding in the series $LiGaX_3$, X = Cl, Br, I, were examined using calculations based on the Extended Hückel Method (EHM) with the parameters and exponents of Table III (*7, 8*). To mimic the change in electronega-

TABLE II

POSITIONAL AND THERMAL PARAMETERS U_{ij} FOR $LiGaCl_3$ (TOP) AND $LiGaI_3$ (BOTTOM)

Atom	x	y	z	U_{eq}	U_{11}	U_{22}	U_{33}	U_{23}	U_{13}	U_{12}
Ga1	0.64210(4)	$\frac{1}{4}$	−0.0842(1)	212(2)	169(3)	247(4)	219(3)	0	5(2)	0
Ga2	0.49380(4)	$\frac{1}{4}$	0.0500(1)	205(2)	165(3)	228(4)	221(3)	0	0(2)	0
Cl11	0.1563(1)	$\frac{1}{4}$	−0.0545(2)	279(4)	303(8)	324(8)	208(7)	0	−1(6)	0
Cl22	0.3880(1)	$\frac{1}{4}$	−0.2045(3)	282(4)	233(7)	291(8)	322(8)	0	−100(6)	0
Cl1	0.72043(7)	04270(1)	0.0472(2)	287(3)	268(5)	292(5)	299(5)	−60(4)	31(4)	−80(4)
Cl2	0.46702(7)	0.0675(1)	0.2647(2)	284(3)	303(5)	279(5)	272(5)	55(4)	11(4)	−24(4)
Li	0.1326(6)	0.5120(11)	0.1167(20)	487(32)	365(46)	499(58)	598(60)	38(49)	−8(42)	−34(44)
Ga1	0.2434(2)	$\frac{1}{4}$	0.8674(2)	245(5)	164(8)	317(7)	256(8)	0	17(6)	0
Ga2	0.9716(2)	$\frac{1}{4}$	0.9664(2)	246(5)	176(9)	322(7)	240(8)	0	10(6)	0
I11	0.4521(1)	$\frac{1}{4}$	0.1420(1)	328(3)	276(6)	406(6)	295(5)	0	−82(4)	0
I22	0.9337(1)	$\frac{1}{4}$	0.3264(1)	316(3)	401(7)	337(5)	212(5)	0	12(4)	0
I2	0.32075(9)	0.07091(6)	0.6609(1)	308(2)	297(5)	339(4)	286(4)	−58(2)	7(3)	33(3)
I2	0.81678(9)	0.06975(6)	0.8251(1)	320(3)	266(5)	401(4)	296(4)	−74(3)	35(3)	−83(3)
Li1	0	0	$\frac{1}{2}$	638(135)	346(205)	773(235)	797(256)	−193(206)	48(185)	−219(184)
Li2	$\frac{1}{2}$	0	0	664(142)	446(235)	607(202)	931(292)	−9(200)	−85(212)	204(181)

Note. The U_{ij} parameters are expressed in the form $\exp[-2\pi^2(U_{11}h^2a^{*2} + \cdots + 2U_{12}hka^*b^*]$ and given in units pm^2. Standard deviations in ( ).

tivity of the three halides, we simply substituted the energies (the H_{ii} values) of the respective *ns* and *np* orbitals of Br and I for those of Cl. We kept the atomic "size" constant for the halide component by only using the orbital exponents of Cl. The following geometrical parameters were selected for the Ga_2X_6 moiety: d(Ga–Ga) = 240 pm, d(Ga–X) = 224 pm, and the (X–Ga–Ga) angle of 109.47° with D_{3h} point symmetry.

6. Discussion

Figure 1 shows the primary structural building units of the $LiGaX_3$ compounds, namely, the eclipsed $Ga_2X_6^{2-}$ dianion and the LiX_6 octahedra. Table IV gives bond distances and pertinent bond angles for both compounds (X = Cl, I). The crystal structure determinations indicate that $LiGaCl_3$ crystallizes in a new structure type, whereas $LiGaI_3$ is isotypic to $LiGaBr_3$, which was formerly described in Ref. (*1*).

The two structures differ primarily in their spatial arrangements of the trigonal prisms [Ga_2X_6] with respect to each other. $LiGaCl_3$ can be regarded as constructed of $LiGaBr_3$-type slabs running along the [100] and [$\bar{1}$00] directions (Fig. 2). To transform one type into the other, a cooperative rotation of one-half of the trigonal prisms [Ga_2Br_6] is necessary. We have previously shown that a group–subgroup relationship exists between $GdFeO_3$ and $LiGaBr_3$ (*1*). In principle, one could think of a similar relationship between the $LiGaCl_3$ and $LiGaBr_3$ structure types as well. However, the required reorientation of one-half of the trigonal prisms does not account for such a clear group–subgroup relationship.

The Li atoms occupy the octahedral holes in $LiGaCl_3$, but in a different arrange-

TABLE III

ATOMIC ORBITAL ENERGIES AND COEFFICIENTS USED IN THE EHM CALCULATIONS

Atom	Orbital	H_{ii}(eV)	ζ
Cl	3*s*	−26.3	2.183
	3*p*	−14.2	1.733
Br	4*s*	−22.07	2.588
	4*p*	−13.10	2.131
I	5*s*	−18.0	2.679
	5*p*	−12.7	2.322
Ga	4*s*	−14.58	1.77
	4*p*	−6.75	1.55

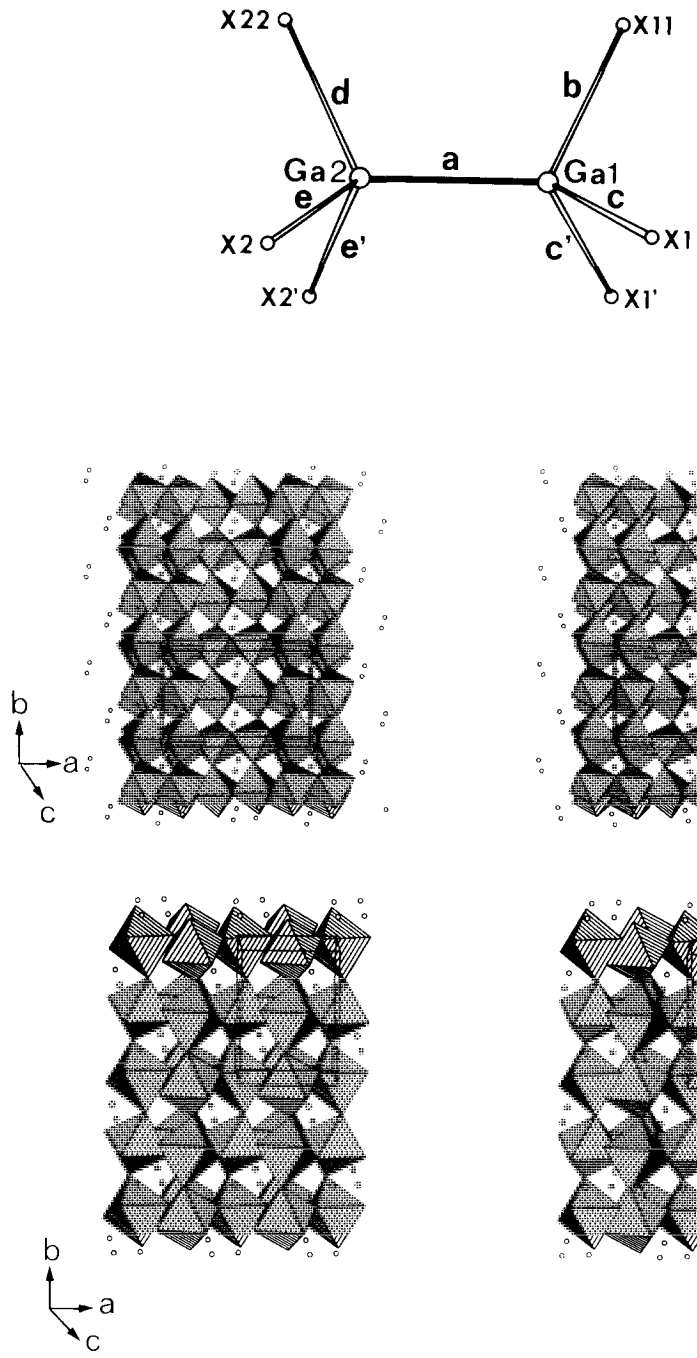

FIG. 1. (Top) Atomic labeling in the Ga_2X_6 unit; (center) stereo view of the $LiCl_6$ octahedral arrangement in $LiGaCl_3$, drawn with STRUPLOT (9); (bottom) stereo view of the LiI_6 octahedral arrangement in $LiGaI_3$, drawn with STRUPLOT (9).

TABLE IV

BOND DISTANCES (PM, TOP) AND BOND ANGLES (DEG, BOTTOM) FOR $LiGaCl_3$ (LEFT) AND $LiGaI_3$ (RIGHT)

	$Ga_2X_6^{2-}$ dianion			LiX_6 octahedra			
Type	Ga	X = Cl	X = I	Atom	Li–Cl	Li1–I	Li2–I
	–Ga1–						
a	Ga2	239.1(1)	242.8(2)	*X*11	278.0(11)	—	304.9(1)*
b	*X*11	222.6(2)	259.7(2)	*X*22	258.1(11)	314.5(1)*	—
c	X1	224.1(1)*	260.9(1)*	*X*1	251.2(10)	302.5(1)*	292.9(1)*
	–Ga2–			*X*1′	258.8(10)	—	—
a	Ga1	239.1(1)	242.8(2)	*X*2	268.8(10)	293.8(1)*	309.6(1)*
d	*X*22	223.7(2)	259.7(2)	*X*2′	272.3(10)		
e	*X*2	224.8(1)*	261.8(1)*				
a–*b*	Ga2–Ga1–*X*11	115.6(1)	114.2(1)		Bond Angles (Li–*X*–Li′)		
a–*d*	Ga1–Ga2–*X*22	115.6(1)	115.8(1)	Li–Cl11–Li′	133.0(4)	Li2–I11–Li2′	137.6(1)
a–*c*	Ga2–Ga1–*X*1	111.9(1)*	114.9(1)*	Li–Cl1–Li′	134.3(3)	Li1–I1–Li2′	132.5(1)
a–*e*	Ga1–Ga2–*X*2	111.8(1)*	110.8(1)*	Li–Cl22–Li′	127.6(5)	Li1–I22–Li1′	129.4(1)
c–*c*′	*X*1–Ga1–*X*1′	100.5(1)	102.6(1)	Li–Cl2–Li′	104.2(3)	Li1–I2–Li2	137.2(1)
e–*e*′	*X*2–Ga2–*X*2′	104.4(1)	103.1(1)		Ranges of angles at Li atoms		
b–*c*	*X*11–Ga1–*X*1	107.9(1)*	104.4(1)*	Li: 75.8–99.7°; 117.6–177.0°		Li1: 83.2–91.5°; 180°	
d–*e*	*X*22–Ga2–*X*2	106.2(1)*	107.7(1)*			Li2: 86.9–91.7°; 180°	

Note. Standard deviations in ( ). For the labeling of the bonds, cf. Fig. 1.
* Indicates multiplicity 2.

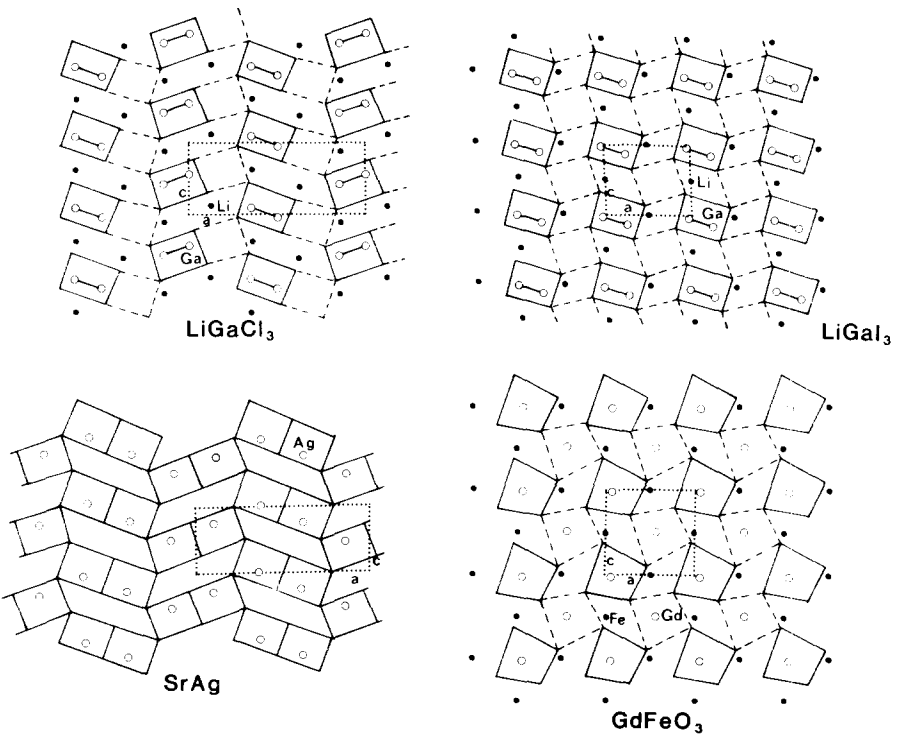

FIG. 2. Comparison of the stacking of trigonal prisms in $LiGaCl_3$ and SrAg (left) and $LiGaI_3$ and $GdFeO_3$ (right).

TABLE V

COMPILATION OF $\bar{d}$(Ga–Ga) AND $\bar{d}$(Ga–X) IN GALLIUM HALIDES (DISTANCES IN PM)

Compound	$\bar{d}$(Ga–Ga)	$\bar{d}$(Ga–X)	Conformation	Reference
$(NMe_4)_2Ga_2Cl_6$	239.0	219.6	Staggered	(*14*)
$(NPr_4)_2Ga_2Br_6$	241.0	236.2	Staggered	(*3*)
Ga_2Br_3	243.3	240.4	Eclipsed	(*2*)
Ga_2I_3	238.8	259.7	Staggered	(*15*)
$LiGaCl_3$	239.1	224.0	Eclipsed	This work
$LiGaBr_3$	240.4	238.9	Eclipsed	(*1*)
$LiGaI_3$	242.8	260.8	Eclipsed	This work

ment from that found in $LiGaBr_3$. Two octahedra form Li_2Cl_{10} units as in $LiGaBr_4$ (*1*), but these units are then connected via their corners to form $[Li_2Cl_{2/1}Cl_{8/2}] \cong [LiCl_3]$ entities. The spatial arrangement of these Li_2Cl_{10} groups corresponds to the γ-MnO_2 structural type (*10*).

The sizes of the thermal ellipsoids of Li display an interesting increase in magnitude. Upon forming the ratios, U(Li)/U(X) and U(Ga)/U(X), which accounts for errors introduced, e.g., by absorption corrections, etc., we find that U(Ga)/U(X) is nearly constant with values of 0.74, 0.72, and 0.77 for X = Cl, Br, I, respectively. The increase of U(Li)/U(X) from 1.72 and 1.63 for X = Cl, Br to 2.05 for X = I indicates an increasing motion of the Li atom in the X_6 octahedra as observed in the $LiGaX_4$ compounds (*11*). The average ratio of U(Ga)/U(X), 0.74, is comparable to that of the $LiGaX_4$ compounds (0.75), which indicates similar amplitudes of the Ga vibration within the homonuclear X_4 as well as the heteronuclear GaX_3 tetrahedron.

Since we have already discussed the Li $GaBr_3$ structure in detail, we will focus here mainly on the structural relationships between $LiGaCl_3$ and other structures. During the evaluation of Fig. 3b in Ref. (1), we deduced the stacking possibilities of the trigonal prisms (TP). When our view is restricted to one layer of TP's, Fig. 2 shows the relationship to $GdFeO_3$, which is a more distorted variant of the $\square SiYPd_2$ structure type. On the other hand, $\square SiYPd_2$ can be regarded as a $\square CFe_3$ variant (*12*). These structure types are directly related to LiGa Br_3, thus leaving one TP empty and occupying the other TP with the Ga–Ga dumbbell. A similar relationship exists for Li $GaCl_3$ if one considers the empty TP and restricts to one layer of TP (and thus accounts for the different stoichiometry). The TP's in $LiGaCl_3$ are arranged in the same way as in the intermetallic compound SrAg (shown in Fig. 2) (*13*). Even the (a/c) ratios (SrAg: 2.59; $LiGaCl_3$: 2.47), (c/b) ratios (SrAg: 1.33; $LiGaCl_3$: (2c/b) = 1.26) support these geometrical considerations as well. Therefore, one can think of possible structure variants within the Li/Ga/X system, like those already determined for the FeB/CrB stacking possibilities (*12*). Variations of the alkali metal cations as well as the halide anions may stabilize other stacking variants.

Regarding the isotypic series $Ga_2X_6^{2-}$ (X = Cl, Br, I), there are two other geometrical features we wish to consider in further detail. These characteristics are listed in Table V, which gives a compilation of $\bar{d}$(Ga–Ga) and $\bar{d}$(Ga–X) in $Ga_2X_6^{2-}$ units as well as the conformation of the halide ligands that are known to date from single crystal determinations. In the $LiGaX_3$

structures, the arrangement of the halide ligands around the Ga–Ga bond adopts an eclipsed conformation as opposed to a completely staggered geometry that is found in the isoelectronic structures of $[P_2S_6^{4-}]$,[16] $[Si_2Te_6^{6-}]$,[17] and ethane. Second, as X proceeds from Cl to Br to I, the Ga–Ga bond distance increases monotonically. This trend of cation-cation distances could be simply attributed to the size of the matrix around the Ga_2 unit and has been observed in further examples, e.g., the tetrahalides of Nb (*18*).

This effect cannot be completely separated from an electronic one, which can even lead to opposite behavior as in the compounds Mo_6Y_8 (Y = S, Se, and Te). Such observations have stimulated several investigations concerning the so-called matrix effect (*19, 20, 21*). Band structure calculations for these chalcogenides have shown that as the chalcogen varies from S to Te, more electrons are transferred into bonding levels of the Mo_6 unit, thereby shortening the Mo–Mo bond lengths (*22*). Furthermore, replacement of Mo atoms by more electron-rich atoms, e.g., Re or Ru, similarly shortens the metal–metal distances within the cluster (*21*).

In the case of the $LiGaX_3$ series of compounds, the GaX_3 fragments approach each other to an extent that the edges parallel to the pseudo-threefold axis of the resulting prism are significantly longer than twice the van der Waals radii of the X atoms (432.6 and 2 × 406.4 pm for Cl, 441.7 and 2 × 443.4 pm for Br, and 455.7 and 2 × 462.5 pm for I compared to 363, 390, and 432, respectively). Therefore, from geometrical arguments concerning only the anion matrix, the Ga–Ga distances could be even shorter than observed. The interactions between the two Ga atoms in the Ga_2 unit seems to control the extent of approach of the two GaX_3 fragments. Furthermore, we suggest that the observed sequence in Ga–Ga bond lengths in this series of compounds are influenced by both the electronic properties of the Ga–Ga dimer as well as the halide, which we have examined using EHM. Although EHM has been demonstrated to be unreliable for predicting internuclear distances via geometry optimizations, it has been reliable in predicting bond length *trends* using comparative overlap populations for idealized geometries.

TABLE VI

CALCULATED OVERLAP POPULATIONS AND MULLIKEN POPULATIONS FOR THE σ AND σ^* LEVELS IN THE Ga–Ga UNIT WITHIN THE $(Ga_2X_6)^{2-}$ (X = Cl, Br, I) FRAGMENT

$Ga_2X_6^{2-}$	p(Ga–Ga)	$q(\sigma)$	$q(\sigma^*)$
Cl	0.8997	2.5685	0.6409
Br	0.8669	2.6327	0.7484
I	0.8517	2.6546	0.8323

Prior to discussing this bond length trend, we wish to point out that the (Ga–Ga–X) angle in all three trigonal prismatic units exceeds the ideal tetrahedral angle by 3° to 6°. EHM calculations on the isolated prisms predicts this angle to be approximately 116° in all three cases. We can attribute this larger angle partly to anion–anion repulsions within the prism, because when we arbitrarily turn off the anion–anion orbital interactions between the two GaX_3 fragments, the predicted (Ga–Ga–X) angle then approaches the tetrahedral angle (109.47°). Therefore, we cannot neglect the influence of anion–anion interactions in controlling the geometry of these $Ga_2X_6^{2-}$ units. For now, we return to the trend in Ga–Ga distances.

Table VI shows that the sequence of overlap populations for the Ga–Ga interaction parallels the trend in bond lengths (smaller overlap populations translate into larger bond distances). We can understand this result qualitatively by examining the interaction between the Ga–Ga dimer with the X_6 trigonal prism. In Table VI we also

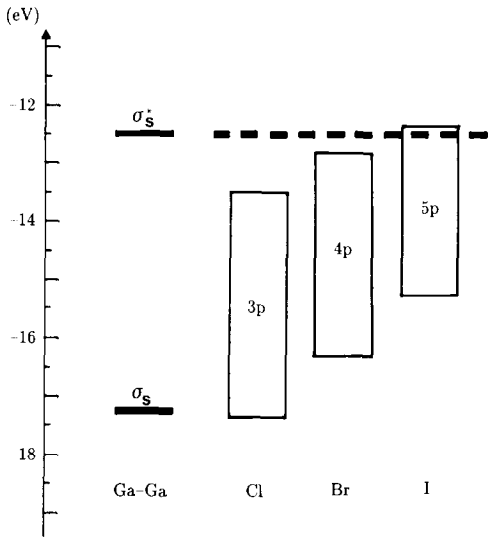

FIG. 3. Relative energies of the σ_s and σ_s^* levels of the Ga–Ga dimer with respect to the p orbital manifolds of the X_6 trigonal prisms.

list the calculated charges (using a Mulliken population analysis) in the σ and σ^* orbitals of the Ga_2 fragment since the HOMO for the $Ga_2X_6^{2-}$ species has σ-type symmetry between Ga atoms. Note that both the σ bonding and σ^* antibonding contributions increase from the chloride to the iodide, of which the σ^* component increases at a much greater rate. As the electronegativity of the halide decreases, the corresponding fragment orbitals of the X_6 prism begin to energetically span both the σ_s and σ_s^* orbitals of the Ga–Ga dimer, as shown in Fig. 3. Since the mixing coefficient of a given fragment orbital into the final molecular orbital is inversely proportional to the energy separation of the two orbitals involved in the interaction, the figure readily illustrates how the contribution from the σ_s^* components gradually increases from Cl to Br to I and, thus, lengthens the Ga–Ga bond distance. Unlike the molybdenum chalcogenides, variation of the anionic constituent from Cl to I transfers more electrons into antibonding levels of the Ga–Ga unit.

The Ga–Ga bond lengths are also sensitive to the (X-Ga–Ga) angle, since the overlap population between Ga atoms decreases as this angle increases from the tetrahedral angle (109.5°). The halides on the triangular faces of the prism move closer together, and begin to widen the energy range of the p-block orbitals (see Fig. 3). The interaction between the Ga–Ga dimer with the X_6 prism then produces an increased contribution from the Ga–Ga σ_s^* orbital. Perhaps this result indicates the reason for the difference in Ga–Ga distances in the two compounds, $LiGaBr_3$ and $GaGaBr_3$ (Table V), which have a similar eclipsed conformation.

The second question regards the relative stability of the staggered geometry for the $Ga_2X_6^{2-}$ fragments, since the eclipsed conformation is observed for all $LiGaX_3$ structures. We should mention that in Ga_2Br_3 the dianion unit is eclipsed, whereas it is staggered in Ga_2I_3 (Table V). EHM calculations on the transformation from staggered to eclipsed geometries determine rotational barriers of 3.8, 1.3, and 3.4 kJ/mole for the chloride, bromide, and iodide, respectively, with the staggered conformation always preferred. This result suggests the importance of the Li–X interactions in controlling the local geometry at each Ga–Ga dimer. Perhaps under higher pressures, the staggered conformation will be observed in order to minimize anion–anion repulsions within the dianion fragment.

Acknowledgments

Our thanks are due to cand. Ing. H. Rothfuß, W. Röthenbach, and Dr. K. Peters (MPI, Stuttgart) for assistance with the preparation, high temperature Guinier photographs, and measurement of the intensities, respectively.

References

1. W. HÖNLE AND A. SIMON, *Z. Naturforsch. B: Anorg. Chem. Org. Chem.* **41B,** 1391 (1986).

2. W. HÖNLE, G. GERLACH, W. WEPPNER, AND A. SIMON, *J. Solid State Chem.* **61,** 171 (1986).
3. H. J. CUMMING, D. HALL, AND C. E. WRIGHT, *Cryst. Struct. Commun.* **3,** 107 (1974).
4. A. SIMON, *J. Appl. Crystallogr.* **3,** 11 (1970).
5. G. M. SHELDRICK, "SHELXTL, A Program System for Crystal Structure Determination," Cambridge, 1978, unpublished.
6. K. YVON AND W. JEITSCHKO, *Parthé J. Appl. Crystallogr.* **10,** 73 (1977).
7. R. HOFFMANN, *J. Chem. Phys.* **39,** 1397 (1983).
8. J. H. AMMETER, H. B. BÜRGI, J. THIBEAULT, AND R. HOFFMANN, *J. Amer. Chem. Soc.* **100,** 3686 (1978).
9. R. X. FISCHER, *J. Appl. Crystallogr.* **18,** 258 (1985).
10. A. F. WELLS, "Structural Inorganic Chemistry," 5th ed., p. 555, Clarendon Press, Oxford, 1984.
11. W. HÖNLE, B. HETTICH, AND A. SIMON, *Z. Naturforsch. B: Anorg. Chem. Org. Chem.* **42B,** 248 (1987).
12. E. PARTHÉ AND B. CHABOT, *in* "Handbook on the Physics and Chemistry of Rare Earths" (K. A. Gschneider and L. Eyring, Eds.), Vol. 2, North-Holland, Amsterdam, 1979.
13. F. MERLO AND M. L. FORNASINI, *Acta Cryst. Sect. B: Struct. Crystallogr. Cryst. Chem.* **B37,** 500 (1981).
14. K. L. BROWN AND D. HALL, *J. Chem. Soc. Dalton,* 1845 (1973).
15. G. GERLACH, W. HÖNLE, AND A. SIMON, *Z. Anorg. Allg. Chem.* **486,** 7 (1982).
16. R. NITSCHE AND P. WILD, *Mater. Res. Bull.* **5,** 419 (1970).
17. G. DITTMAR, *Acta Cryst. Sect. B: Struct. Crystallogr. Cryst. Chem.* **B34,** 2390 (1978).
18. W. KLEMM, W. BRONGER, AND H.-G. VON SCHNERING, *in* "Jahrbuch 1966," pp. 451–473, Landesamt für Forschung des Landes Nordrhein-Westfalen, Westdeutscher Verlag, Köln/Opladen.
19. K. YVON, *in* "Current Topics in Material Science" (E. Kaldis, Ed.), Vol. 3, p. 53, North-Holland, Amsterdam, 1979.
20. J. D. CORBETT, *J. Solid State Chem.* **39,** 56 (1981).
21. W. HÖNLE, H. D. FLACK, AND K. YVON, *J. Solid State Chem.* **49,** 157 (1983).
22. H. NOHL, W. KLOSE, AND O. K. ANDERSEN, *in* "Superconductivity in Ternary Compounds I" (Ø Fisher and M. B. Maple, Eds.), Springer-Verlag, Berlin, 1982.